ARTICLES
https://doi.org/10.1038/s41558-021-01104-8

nature climate change

Plant pathogen infection risk tracks global crop yields under climate change

Thomas M. Chaloner[1], Sarah J. Gurr[1,2] and Daniel P. Bebber[1]✉

Global food security is strongly determined by crop production. Climate change-induced losses to production can occur directly or indirectly, including via the distributions and impacts of plant pathogens. However, the likely changes in pathogen pressure in relation to global crop production are poorly understood. Here we show that temperature-dependent infection risk, *r*(*T*), for 80 fungal and oomycete crop pathogens will track projected yield changes in 12 crops over the twenty-first century. For most crops, both yields and *r*(*T*) are likely to increase at high latitudes. In contrast, the tropics will see little or no productivity gains, and *r*(*T*) is likely to decline. In addition, the United States, Europe and China may experience major changes in pathogen assemblages. The benefits of yield gains may therefore be tempered by the greater burden of crop protection due to increased disease and unfamiliar pathogens.

Plant pests and pathogens exert a major burden on crop production around the world[1]. The burden can be measured directly in yield losses or indirectly in the social, environmental and economic costs of control[1]. Like all species, crop pests and pathogens have particular tolerances to or requirements for particular environmental conditions[2]. These tolerances define their ecological niche, which determines the geographical regions and periods of the year that allow pests and pathogens to proliferate and attack crops[2]. As climate changes, suitable conditions for pest outbreaks shift in time and space, altering the threats that farmers face and the management regimes required for their control[3]. Modelling the patterns and processes of future changes in pest and pathogen burdens is therefore a key component in maintaining future food security[4].

Latitudinal range shifts of pests and pathogens are expected as the planet warms and populations track their preferred temperature zones[3]. Spatial movements in geographical distributions and temporal shifts in phenologies of wild populations are among the clearest signs of anthropogenic global warming[5]. Though distribution data for crop pests and pathogens are noisy and incomplete[4], similar changes have been detected for hundreds of species of pests and pathogens over recent decades[6]. Increasing burdens of insect pests at high latitudes and decreasing burdens at low latitudes have been projected using ecological niche models[7]. These models attempt to reconstruct the environmental tolerances of species from contemporary climates within the observed species range using statistical models[8]. Alternatively, species' responses to microclimates can be directly measured, and these responses can be incorporated into physiologically based models of species performance[9]. Such mechanistic models are commonly used to project future crop yields[10], and models have also been developed for some plant diseases[11,12]. However, we know little about how plant disease pressure is likely to change in the future or how these changes will relate to crop yield responses to climate change.

Infection and disease are determined by complex and species-specific interactions between various biotic and abiotic factors[1]. Temperature is a major determinant of disease risk[2,13], and global distributions of plant pathogens have shifted in line with historical global warming[6]. Here, we analyse temperature response functions for host infection for a suite of fungal and oomycete plant pathogens. We model the likely global shifts in temperature-dependent infection risk, $r(T)$, for the twenty-first century and compare climate-driven changes in this risk with projected changes in crop yields.

Projected crop yield changes

We compared current (2011–2030 mean) and future (2061–2080 mean) yield projections from three crop models (LPJmL, GEPIC and PEPIC) employing four global climate models (GCMs) (GFDL-ESM2M, HADGEM2-ES, IPSL-CM5A-LR and MIROC5) under Representative Concentration Pathway (RCP) 6.0. Carbon dioxide fertilization effects were included, and we compared projections with and without irrigation. Crop models do not explicitly consider the impacts of pests, pathogens and weeds on production. The major commodity crops of maize, wheat, soybean and rice are considered in all three crop models.

Crop models project greater yield increases at higher latitudes, with smaller increases or yield declines at low latitudes[14,15] (Supplementary Figs. 1–4). Under the no irrigation scenario, GEPIC and PEPIC project substantial maize yield declines in Central and Latin America (except for Argentina) and across Africa and northern Australia. LPJmL projects no such yield declines. Wheat yields also increase at high latitudes in all three crop models, with smaller increases at low latitudes in LPJmL and declines in GEPIC and PEPIC. North America and parts of Eurasia show the largest wheat yield increases, while GEPIC projects large declines in yield across the tropics. A similar latitudinal trend is projected for soybean but with little decline in the tropics. Soybean yield increases are projected across Eurasia in all models and also in Argentina and South Africa in GEPIC and PEPIC. The latitudinal gradient is less pronounced for rice, with the MIROC5 climate model suggesting a large increase in yield in the Southern Hemisphere.

Eight further temperate and tropical annual crops are considered in LPJmL. In the unirrigated scenario, cassava yields increase under all four GCMs within 40° of latitude, driven by large increases in India. However, all four GCMs suggest a smaller increase within 10° N, caused by a yield decline in northern Brazil. Peanut, pea, rapeseed,

[1]Department of Biosciences, University of Exeter, Exeter, UK. [2]Department of Biology, Utrecht University, Utrecht, Netherlands.
✉e-mail: d.bebber@exeter.ac.uk

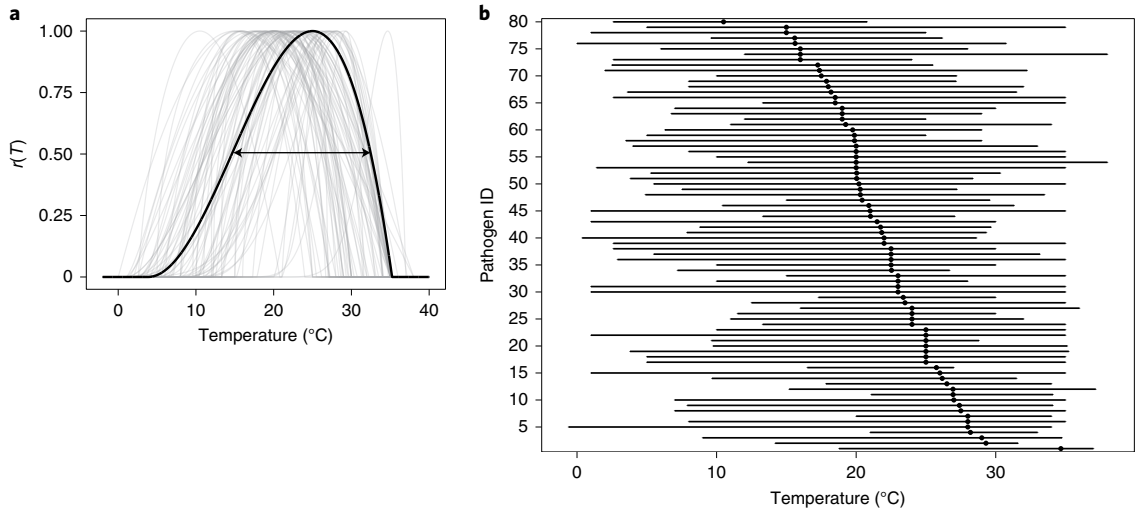

Fig. 1 | Summary of infection cardinal temperatures for 80 plant pathogens included in this study. a, Temperature response curves for $r(T)$ determined by T_{min}, T_{opt} and T_{max}, as well as equation (1). The double-headed arrow refers to temperatures where $r(T) = 0.5$ for an example pathogen (black curve). **b**, The points refer to T_{opt}, and the bars refer to the temperature range (defined by T_{min} and T_{max}). Pathogen IDs are provided in Supplementary Table 1.

sugar beet and sunflower show increases at all latitudes, with the largest increases at higher latitudes. Millet also shows increases at high latitudes, but yield declines at low latitudes. There are no consistent differences among the four GCMs for any of the crops. The results for sugar cane are more variable. Mean yield change projections suggest declines in Brazil and other Latin American countries and in Southeast Asia, but increases in the United States and in East Africa. Previous analyses based on the more extreme RCP 8.5 scenario suggest similar yield increases at high latitudes, but more severe declines for some crops at low latitudes[15].

Total projected crop production change is difficult to estimate because the spatial distributions of planted areas are impossible to predict, due to the influence of socio-economic and cultural factors on planting choice. However, if production is calculated from projected yield changes on an estimate of current crop production, increases in production are expected for many crops (Supplementary Fig. 5). Global wheat, cassava, rapeseed and sunflower production are predicted to increase by all models. LPJmL and two climate models driving GEPIC and PEPIC predict increases for rice. All models except HADGEM2-ES predict global soybean production increases. None of the crop models unequivocally project declines in production for any crop. In summary, crop models project global production increases driven primarily by yield increases at high latitudes, even without changes in cropping patterns to match shifts in areas likely to be most productive.

Projected changes in yield for full irrigation are qualitatively and quantitatively similar to those for no irrigation across latitudes (Supplementary Fig. 6). PEPIC shows substantially greater yield increases in the Southern Hemisphere for several crops. In certain cases, yields decline more at lower latitudes with full irrigation than with no irrigation. This is because irrigation enables cultivation in otherwise-unsuitable land for these crops, in these models. In summary, both irrigated and unirrigated crop model projections suggest positive latitudinal shifts in crop yields over the next half century[14,15].

Projected infection risk changes

Could these yield increases be offset by changing crop disease risk? The infection of plants by pathogens occurs at different rates depending on temperature, and each pathogen has a different optimum temperature at which infection of the host is the most rapid[2]. Infection rates are commonly estimated by quantifying the appearance of disease lesions on host plants under controlled conditions[16]. We estimated relative $r(T)$ of 80 fungal and oomycete plant pathogens for which minimum (T_{min}), optimum (T_{opt}) and maximum (T_{max}) infection temperatures were available in the literature[2] (Fig. 1 and Supplementary Table 1). These rates are relative (bound between zero and one) to enable comparison among pathogens. The rate is greatest—that is, $r(T) = 1$—at T_{opt} and declines to zero as temperature decreases to T_{min} or increases to T_{max}. We chose to model infection temperature responses rather than the more commonly measured growth in culture, because in planta responses differ substantially from in vitro responses[2]. Essentially, the temperature range for infection is narrower and the optimum temperature is lower than for growth in culture. However, for two important pathogens, *Magnaporthe oryzae* (causing rice blast) and *Zymoseptoria tritici* (causing Septoria tritici blotch of wheat), infection temperatures were not available; we therefore used lesion development and growth in culture temperatures, respectively. Optimum infection temperatures varied from 10.5 to 34.7 °C among species (median, 21.9; interquartile range, 19.6–25.0). As global temperatures rise (Supplementary Fig. 7), infection risks (and distributions) of these pathogens should shift latitudinally[3].

We defined pathogen species richness, R_r, as the number of pathogens with $r(T) \geq 0.5$ for their hosts in a particular location (Supplementary Figs. 8 and 9) at a particular time. We found that R_r decreases at low latitudes and increases at high latitudes by the end of the twenty-first century under RCP 6.0 (Fig. 2a,b). R_r increases substantially in Europe and China but declines in Brazil, sub-Saharan Africa, India and Southeast Asia. Rapid global dissemination by international trade and transport[17] means that pathogens are likely to reach all suitable areas that are not yet affected (Supplementary Fig. 10).

In our model, R_r was projected to vary through the year, with the largest increases in North America, Europe and China during Northern Hemisphere autumn (Fig. 3 and Supplementary Fig. 11). Decreases in R_r are projected at low to mid-latitudes in Northern Hemisphere winter, shifting northwards into higher latitudes during summer. India is expected to see large declines in R_r over much of the year, with increases in northern parts of India only in winter. Under increasingly strong GHG emissions scenarios, the overall latitudinal patterns of R_r and resultant compositional change in both hemispheres remain the same, but their amplitudes increase

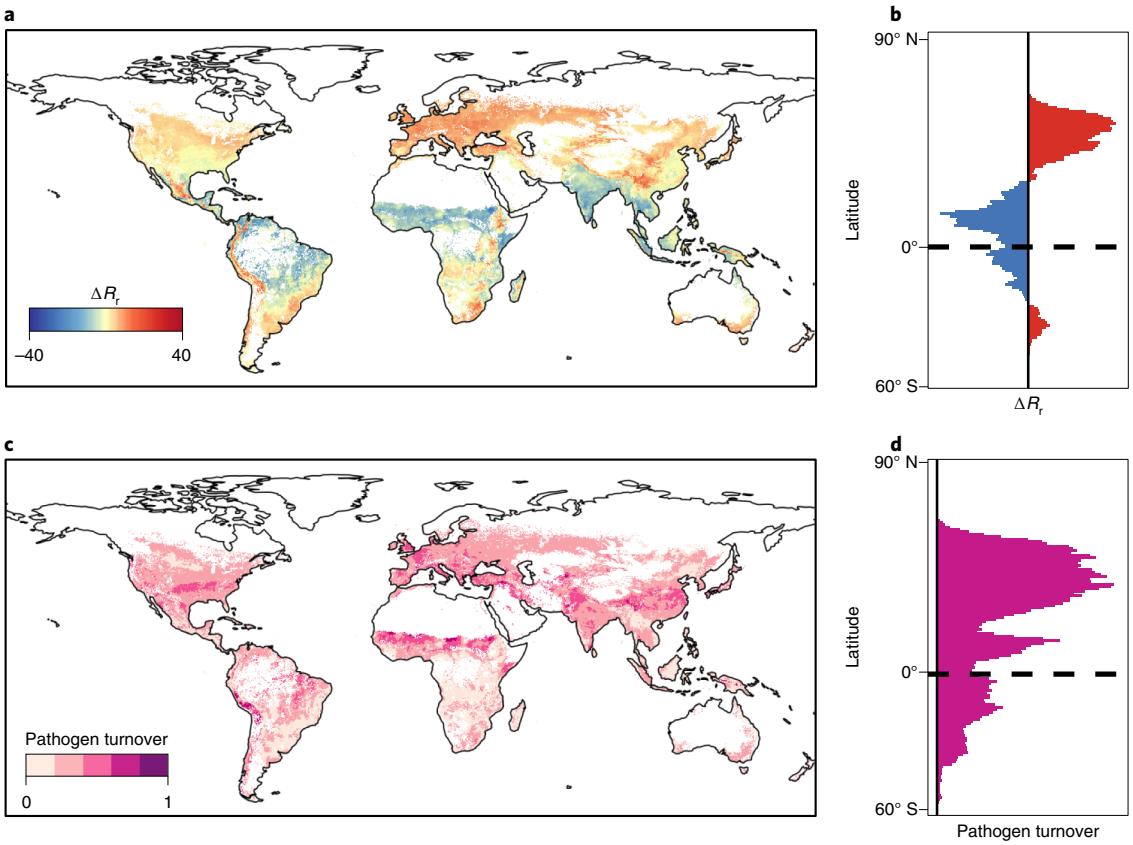

Fig. 2 | Average change in R_r and pathogen turnover under RCP 6.0 across all months. a,**b**, Average change in R_r. **c**,**d**, Average change in pathogen turnover. Red and blue indicate increases and decreases in R_r, respectively. Darker pink indicates larger pathogen turnover. Pathogens are restricted by host distributions extracted from EarthStat[33]. White grid cells contain no hosts and were excluded from the analysis. In **b**,**d**, the data were aggregated to 1° resolution for plotting.

(Fig. 4). R_r declines at low latitudes and increases at high latitudes, while compositional changes peak at around 10° and 30–40°.

Future changes in pathogen $r(T)$ follow changes in yield by latitude for the majority of crops (Fig. 5). Most rice pathogens in our sample show increased $r(T)$ across all latitudes, with few showing a widespread decline in the tropics. While $r(T)$ of several maize pathogens is expected to increase at low latitudes, the risk from many others will decline. Maize, millet and sugar cane are expected to undergo yield declines at low latitudes, but these will be accompanied by declines in $r(T)$ for many of their pathogens. Soybean, sunflower and wheat show little yield gain in the tropics, while experiencing reduced $r(T)$ from a number of pathogens. Conversely, both yields and $r(T)$ increase strongly with latitude. Cassava $r(T)$ generally increases near the Equator. Overall, high latitudes will see increasing potential crop yields while simultaneously facing a larger $r(T)$ by fungal and oomycete pathogens.

We found significant direct spatial matching between future changes in $r(T)$ and crop yields (Supplementary Fig. 12). The correlations between future changes in crop yields and $r(T)$ for maize, soybean, sunflower and wheat exceeded 0.4. Although a weak negative correlation was calculated for cassava (Pearson correlation = −0.09), our analysis included far fewer pathogens for this crop than for other crops (Supplementary Table 2). Future crop production, particularly for three major crops, will probably be affected by climate change not only directly but also indirectly via shifts in plant pathogen distributions.

Changing climate will affect not only the number of pathogens able to infect crops but also the compositions of pathogen assemblages (Fig. 2c,d). Overall, the largest changes in pathogen species composition will occur at high latitudes in the Northern Hemisphere, particularly in Europe, China and the central to eastern United States. Large changes are also expected in the Sahel, but this region, like much of Brazil, India and southeast Asia, will see declines in overall R_r. Hence, the change in pathogen assemblage in these areas is unlikely to pose a major threat to production. Europe, China and Peru are highlighted as regions where both overall burden and species turnover are greatest. These regions will therefore experience the greatest amount of emerging (that is, novel) pathogen pressure. Through the year, two pulses of pathogen assemblage change are seen at high latitudes in the Northern Hemisphere, the first around April and the second around September (Fig. 3). The largest changes in species composition are expected in spring and autumn in the northern United States and Canada, Europe and northern China (Fig. 3 and Supplementary Fig. 13). The largest changes in the Sahel are seen during April and May, while the largest changes in India are seen during May and June.

We compared our model predictions against current known pathogen distributions (Supplementary Fig. 10 and Supplementary Table 3). Restricting predicted distributions by host distributions (EarthStat) improved overall model fit, reducing false positive rates (predicting pathogen presence in regions where the pathogen is currently not reported) and increasing true negative rates (predicting pathogen absence in regions where the pathogen is currently unreported). As in other species distribution models, we predicted areas of suitability and therefore potential distributions of species, and did not attempt to reconstruct observed distributions. Pathogens are spreading globally[17], observational records suf-

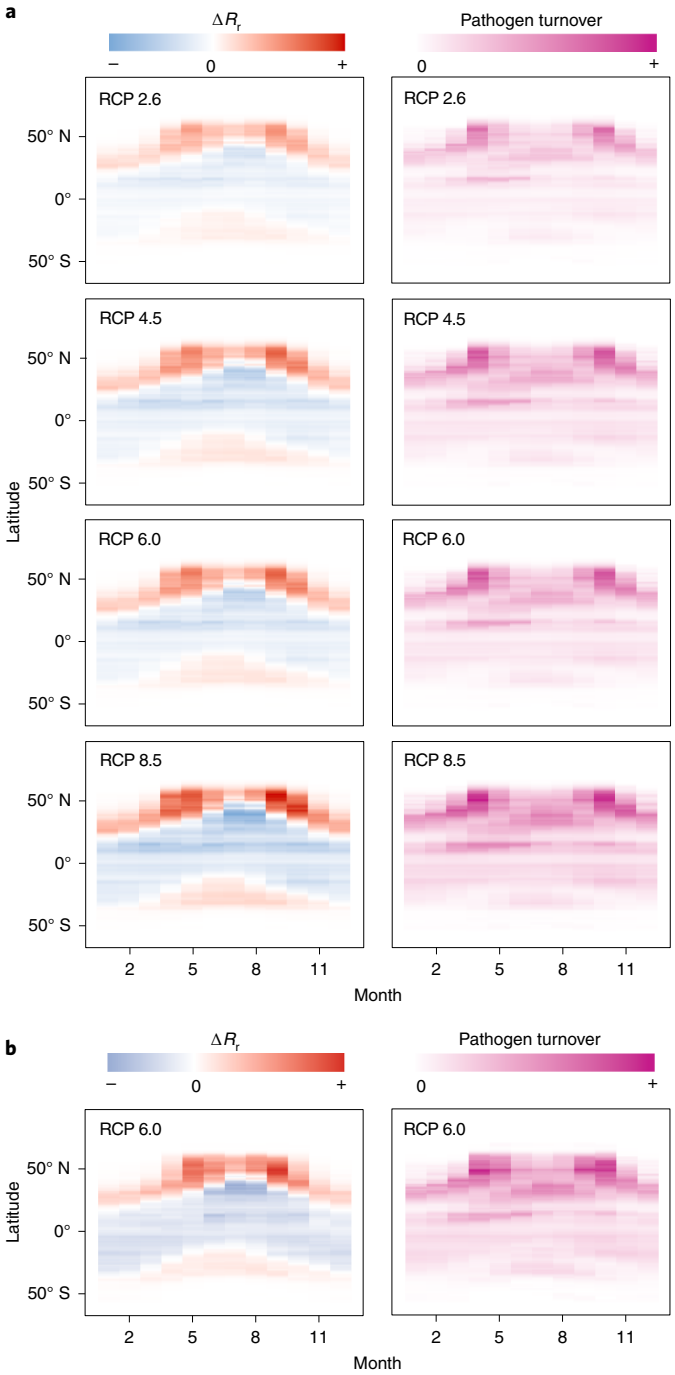

Fig. 3 | Effect of RCP and pathogen restriction method on change in R_r and pathogen turnover. a,**b**, Pathogens are restricted by estimates of host distributions extracted from EarthStat[33] (**a**) and MIRCA2000 (ref. [34]) (**b**). Red and blue indicate increases and decreases in R_r, respectively. Darker pink indicates larger pathogen turnover. Crop calendars were considered only in MIRCA2000. Fewer pathogens are included in **b** because fewer host distributions were available. The data were aggregated to 1° resolution for plotting.

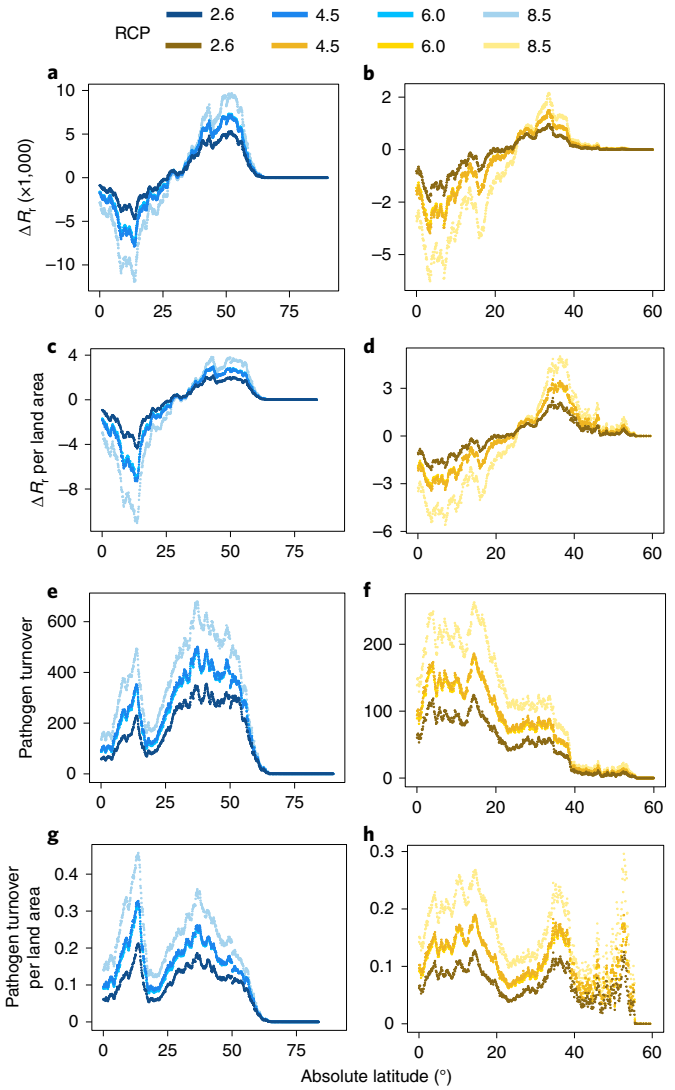

Fig. 4 | Effect of RCP on average change in R_r and pathogen turnover across all months. a–**h**, Change in R_r (**a**–**d**) and pathogen turnover (**e**–**h**) in the Northern Hemisphere (**a**,**c**,**e**,**g**) and the Southern Hemisphere (**b**,**d**,**f**,**h**). Pathogens are restricted by estimates of host distributions extracted from EarthStat. Land area refers to total land area, not crop area.

fer from under-reporting[4] and dispersal limitation prevents species from occupying all possible suitable environments[18]. These factors all probably contributed to the high false positive rates (median, 0.47; interquartile range, 0.37–0.57) of our model. However, high false positive rates were more likely in countries with low per capita gross domestic product (GDP) (Supplementary Fig. 10h), indicating an under-reporting bias in developing countries[4]. Importantly, our model did not erroneously confine potential pathogen distributions, as false negative rates (predicting pathogen absence in regions where the pathogen is currently reported) were very low (median, 0.01; interquartile range, 0.01–0.03).

Discussion

Our analyses are limited by the availability of infection temperature responses in the published literature. These are not a random sample of all known fungal and oomycete plant pathogens. Given that the historical research focus on plant pathogens has been in developed countries at high latitudes[19], our sample is biased towards pathogens that have evolved to infect hosts optimally in cooler climates (Supplementary Fig. 14). However, our sample does include pathogens able to infect both tropical and temperate crops (Supplementary Figs. 8 and 9); hence, this bias does not preclude drawing conclusions for tropical pathogens.

Infection of a susceptible primary host is central to disease development, but other processes such as spore dispersal, overwintering

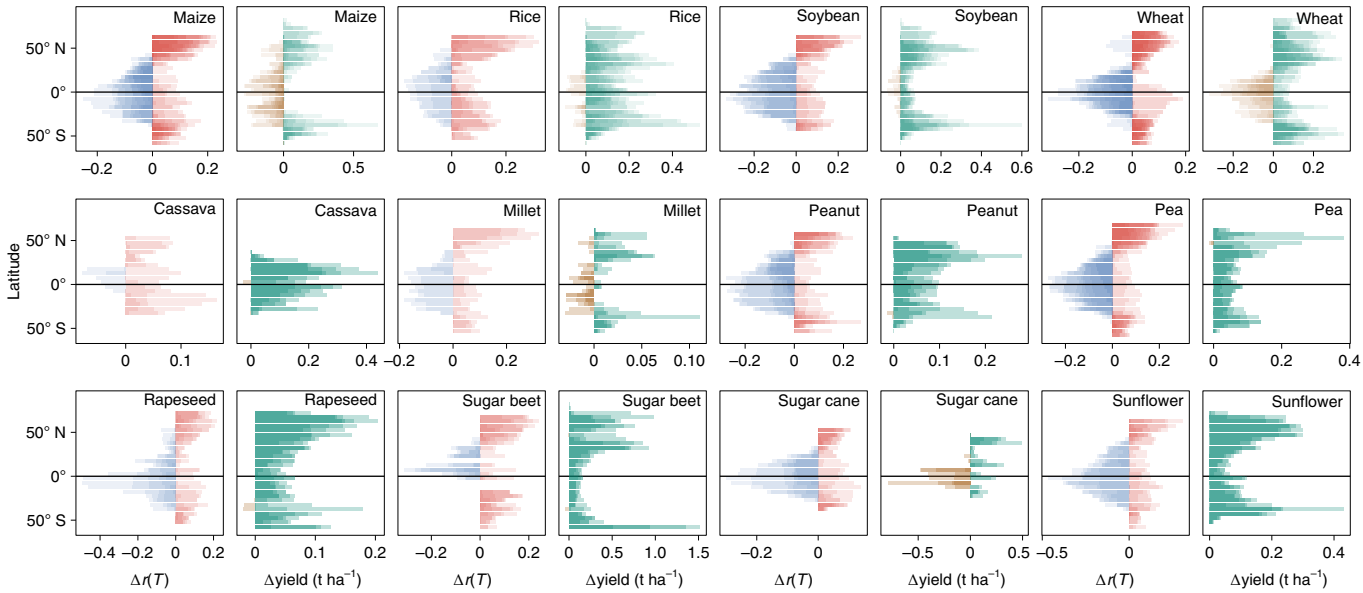

Fig. 5 | Changes in crop yield and *r*(*T*) under RCP 6.0 by latitude. Red and blue indicate increases and decreases in *r*(*T*), respectively. Green and brown indicate increases and decreases in crop yield, respectively, under the no irrigation scenario. Colour saturation indicates the number of pathogens or number of crop and climate models. Pathogens are restricted by estimates of host distributions extracted from MIRCA2000. The data were aggregated to 5° resolution for plotting.

and infection of any alternate hosts are also important in pathogen epidemiology. We have modelled infection only, in common with previous studies on climate change effects on plant pathogens[11,20], under the assumption that inoculum will be present, through either long-distance dispersal or overwintering[21].

We did not attempt to model intraspecific variation in temperature response functions, though such variation does exist[22,23]. However, analysis of historical pathogen distributions indicates that range shifts have occurred in line with expectations, suggesting that temperature adaptation is slow in comparison with climate change[6]. We employed infection temperatures rather than the more commonly measured growth in axenic culture[2] for all but two pathogens, which were included because of their importance in agriculture[1]. The distinction is important because growth in culture has a wider temperature range for most pathogens[2], and models based on growth in culture would suggest a wider geographical range than models based on infection dynamics.

We considered only temperature as a determinant of infection rates. However, infection by many fungal and oomycete plant pathogens is promoted by wet conditions[24]. Multimodel mean projections to the end of the twenty-first century suggest that precipitation will increase significantly in boreal regions and decrease significantly around the Mediterranean, with smaller and less certain changes elsewhere even under a high-emissions scenario[25]. Thus, there seems to be no major change in hydrology that would alter our overall conclusions on latitudinal shifts in pathogen burden. In addition, historical shifts in species populations have largely been driven by global warming[6]. Relative humidity (RH) declines may offset the impact of increased pathogen temperature suitability at higher latitudes, particularly across Europe (Supplementary Fig. 15). Increased plant infection across Europe has been predicted under future climate, where pathogen temperature tolerances and infection wetting period were considered[11]. RH was not considered in our model due to the paucity of data concerning pathogen–RH relations, as well as large uncertainties in future global RH projections[26]. To investigate the consequences of omitting humidity effects on infection risk, we compared the results of models using three-hourly temperature and leaf wetness estimates with those using only three-hourly temperature and only monthly temperature during the growing season, for two rust pathogens (see Appendix in Supplementary Information). We found that the monthly temperature models replicated the overall spatio-temporal patterns seen in the three-hourly temperature and leaf wetness models, and that infection rate estimates were highly correlated among models. Finally, global observations[27] and field-scale experiments[28] suggest that temperature is the most important determinant of fungal distributions and activity.

We did not include potential future changes in crop phenology. Warming is expected to extend the growing season of temperate crops by a few days by the end of the twenty-first century, while increasing temperatures may reduce the length of the growing season in tropical crops[29]. As our seasonal modelling was conducted using monthly crop calendars, the influence of altered growing seasons on our results is likely to be small. We did not include potential future changes in crop distributions. The socio-economic factors leading to changes in future crop distributions are challenging to predict[30], and differing future land use scenarios are beyond the scope of the present analysis. The crop yield projections we employed are subject to uncertainty, both due to the parameterization of the crop models themselves and due to the future climate change scenarios[31,32]. However, the global pattern of greater yield increases at higher latitudes is conserved across models and accords with the latitudinal trends in temperature.

Future crop yields have been modelled using only plant physiological responses to abiotic conditions. We analysed pathogen temperature physiology to understand how indirect, biotic responses to climate change could impact production. We have shown that crop disease burdens could track crop responses, increasing at higher latitudes where climate change is projected to boost yields. Furthermore, the suite of crop diseases that farmers face in some of the world's most productive regions will change dramatically. Crop yield losses to pathogens depend on many factors beyond infection, such as host resistance and crop protection[1]. Agriculture must therefore prepare accordingly if any potential benefits of climate change for crop yields are to be realized.

Online content

Any methods, additional references, Nature Research reporting summaries, source data, extended data, supplementary information, acknowledgements, peer review information; details of author contributions and competing interests; and statements of data and code availability are available at https://doi.org/10.1038/s41558-021-01104-8.

Received: 28 April 2020; Accepted: 29 June 2021;
Published online: 5 August 2021

References

1. Fones, H. N. et al. Threats to global food security from emerging fungal and oomycete crop pathogens. *Nat. Food* **1**, 332–342 (2020).
2. Chaloner, T. M., Gurr, S. J. & Bebber, D. P. Geometry and evolution of the ecological niche in plant-associated microbes. *Nat. Commun.* **11**, 2955 (2020).
3. Bebber, D. P. Range-expanding pests and pathogens in a warming world. *Annu. Rev. Phytopathol.* **53**, 335–356 (2015).
4. Bebber, D. P. et al. Many unreported crop pests and pathogens are probably already present. *Glob. Change Biol.* **25**, 2703–2713 (2019).
5. Parmesan, C. Ecological and evolutionary responses to recent climate change. *Annu. Rev. Ecol. Syst.* **37**, 637–669 (2006).
6. Bebber, D. P., Ramotowski, M. A. T. & Gurr, S. J. Crop pests and pathogens move polewards in a warming world. *Nat. Clim. Change* **3**, 985–988 (2013).
7. Yan, Y., Wang, Y.-C., Feng, C.-C., Wan, P.-H. M. & Chang, K. T.-T. Potential distributional changes of invasive crop pest species associated with global climate change. *Appl. Geogr.* **82**, 83–92 (2017).
8. Elith, J. & Leathwick, J. R. Species distribution models: ecological explanation and prediction across space and time. *Annu. Rev. Ecol. Evol. Syst.* **40**, 677–697 (2009).
9. Kearney, M. & Porter, W. Mechanistic niche modelling: combining physiological and spatial data to predict species' ranges. *Ecol. Lett.* **12**, 334–350 (2009).
10. Bondeau, A. et al. Modelling the role of agriculture for the 20th century global terrestrial carbon balance. *Glob. Change Biol.* **13**, 679–706 (2007).
11. Bregaglio, S., Donatelli, M. & Confalonieri, R. Fungal infections of rice, wheat, and grape in Europe in 2030–2050. *Agron. Sustain. Dev.* **33**, 767–776 (2013).
12. Bebber, D. P. Climate Change effects on Black Sigatoka disease of banana. *Philos. Trans. R. Soc. B* **374**, 20180269 (2019).
13. Delgado-Baquerizo, M. et al. The proportion of soil-borne pathogens increases with warming at the global scale. *Nat. Clim. Change* **10**, 550–554 (2020).
14. Ostberg, S., Schewe, J., Childers, K. & Frieler, K. Changes in crop yields and their variability at different levels of global warming. *Earth Syst. Dyn.* **9**, 479–496 (2018).
15. Rosenzweig, C. et al. Assessing agricultural risks of climate change in the 21st century in a global gridded crop model intercomparison. *Proc. Natl Acad. Sci. USA* **111**, 3268–3273 (2014).
16. Magarey, R. D., Sutton, T. B. & Thayer, C. L. A simple generic infection model for foliar fungal plant pathogens. *Phytopathology* **95**, 92–100 (2005).
17. Bebber, D. P., Holmes, T. & Gurr, S. J. The global spread of crop pests and pathogens. *Glob. Ecol. Biogeogr.* **23**, 1398–1407 (2014).
18. Soberón, J. & Nakamura, M. Niches and distributional areas: concepts, methods, and assumptions. *Proc. Natl Acad. Sci. USA* **106**, 19644–19650 (2009).
19. Bebber, D. P., Holmes, T., Smith, D. & Gurr, S. J. Economic and physical determinants of the global distributions of crop pests and pathogens. *N. Phytol.* **202**, 901–910 (2014).
20. Sparks, A. H., Forbes, G. A., Hijmans, R. J. & Garrett, K. A. Climate change may have limited effect on global risk of potato late blight. *Glob. Change Biol.* **20**, 3621–3631 (2014).
21. Chen, X. M. Epidemiology and control of stripe rust [*Puccinia striiformis* f. sp. *tritici*] on wheat. *Can. J. Plant Pathol.* **27**, 314–337 (2005).
22. Zhan, J. & McDonald, B. A. Thermal adaptation in the fungal pathogen *Mycosphaerella graminicola*. *Mol. Ecol.* **20**, 1689–1701 (2011).
23. Robin, C., Andanson, A., Saint-Jean, G., Fabreguettes, O. & Dutech, C. What was old is new again: thermal adaptation within clonal lineages during range expansion in a fungal pathogen. *Mol. Ecol.* **26**, 1952–1963 (2017).
24. Rowlandson, T. et al. Reconsidering leaf wetness duration determination for plant disease management. *Plant Dis.* **99**, 310–319 (2014).
25. IPCC *Climate Change 2013: The Physical Science Basis* (eds Stocker, T. F. et al.) (Cambridge Univ. Press, 2013).
26. Dunn, R. J. H., Willett, K. M., Ciavarella, A. & Stott, P. A. Comparison of land surface humidity between observations and CMIP5 models. *Earth Syst. Dyn.* **8**, 719–747 (2017).
27. Větrovský, T. et al. A meta-analysis of global fungal distribution reveals climate-driven patterns. *Nat. Commun.* **10**, 5142 (2019).
28. Liu, X. et al. Warming affects foliar fungal diseases more than precipitation in a Tibetan alpine meadow. *N. Phytol.* **221**, 1574–1584 (2019).
29. IPCC *Climate Change 2014: Impacts, Adaptation, and Vulnerability* (eds Field, C. B. et al.) (Cambridge Univ. Press, 2014).
30. Sohl, T. L., Wimberly, M. C., Radeloff, V. C., Theobald, D. M. & Sleeter, B. M. Divergent projections of future land use in the United States arising from different models and scenarios. *Ecol. Model.* **337**, 281–297 (2016).
31. Müller, C. et al. Exploring uncertainties in global crop yield projections in a large ensemble of crop models and CMIP5 and CMIP6 climate scenarios. *Environ. Res. Lett.* **16**, 034040 (2021).
32. Folberth, C. et al. Parameterization-induced uncertainties and impacts of crop management harmonization in a global gridded crop model ensemble. *PLoS ONE* **14**, e0221862 (2019).
33. Monfreda, C., Ramankutty, N. & Foley, J. A. Farming the planet: 2. Geographic distribution of crop areas, yields, physiological types, and net primary production in the year 2000. *Glob. Biogeochem. Cycles* **22**, GB1022 (2008).
34. Portmann, F. T., Siebert, S. & Döll, P. MIRCA2000—global monthly irrigated and rainfed crop areas around the year 2000: a new high-resolution data set for agricultural and hydrological modeling. *Glob. Biogeochem. Cycles* **24**, 1–24 (2010).

Methods

Model summary. A workflow detailing data preparation, model construction, model validation against known pathogen distributions and RH considerations is presented in Supplementary Fig. 16.

Crop yields. Annual crop yield projections from 2006–2099 were obtained from the Inter-Sectoral Model Intercomparison Project (www.isimip.org) in January 2020. The crop models were LPJmL[10], GEPIC[35] and PEPIC[36]. LPJmL simulates changes in the carbon and water cycles due to land use, phenology, seasonal CO_2 fluxes and crop production. GEPIC and PEPIC are derived from the EPIC agricultural yield and water quality model[37]. In EPIC, potential crop yield is simulated from solar radiation, crop parameters, leaf area index and harvest index (the economic yield per unit aboveground biomass). Each of these crop models was driven by four GCMs: MIROC5 (ref. [38]), HadGEM2-ES[39], GFDL-ESM2M[40] and IPSL-CM5A-LR[41]. Annual crop yield estimates under RCP 6.0, with CO_2 fertilization effects, and both the 'no irrigation' and 'full irrigation' scenarios, were obtained for all available crops at 0.5° spatial resolution. Fertilizer application rates are modelled at the country scale in each model. Irrigation is modelled using estimates of the area equipped for irrigation per grid cell. GEPIC and PEPIC modelled maize, rice, soybean and wheat. LPJmL additionally included cassava, millet, pea, peanut, rapeseed, sugar beet, sugar cane and sunflower. Yield differences between the 2060–2080 mean and the 2010–2030 mean were calculated per grid cell.

Climate data. Global estimates of recent (1970–2000 average) and future (2061–2080 average) average monthly temperature at five-arc-minute spatial resolution were obtained from the WorldClim database (www.worldclim.org). For future estimates, all GCMs of RCPs 2.6, 4.5, 6.0 and 8.5 were obtained (Supplementary Table 4). For each RCP–GCM combination, the average future monthly temperature was calculated as the midpoint of the average maximum and minimum monthly temperatures, as no average estimates were available. For each RCP, the average monthly temperature was calculated as the mean of all GCMs for that RCP.

Pathogen dataset construction. Estimates of pathogen infection cardinal temperature were extracted from two sources[16,42]. Collectively, only pathogens with at least one minimum (T_{min}), optimum (T_{opt}) and maximum (T_{max}) estimate for infection cardinal temperature were included. To aid matching of species between sources, pathogen species names reported in the sources were updated according to the Species Fungorum Database (SFD) (www.speciesfungorum.org) (Supplementary Table 5). If no information was available in the SFD, Mycobank (www.mycobank.org) was used as an alternative. Discovery and sanction author(s) of species were not provided in one source[16] and are not considered here. Pathogen species names have previously been processed[42] and so were not altered. Mean T_{min}, T_{opt} and T_{max} were calculated for each pathogen (hereafter referred to as the 'Pathogen dataset'). Pathogens with nonsensical cardinal temperatures (that is, mean T_{opt} > mean T_{max}) were excluded from the analysis, as it was not possible to calculate temperature response functions for such pathogens. *M. oryzae* and *Z. tritici* are two of the most destructive pathogens of rice and wheat[1], respectively, but infection temperature estimates are unavailable. We therefore included cardinal temperature for lesion development of *M. oryzae*[43] and average growth in culture cardinal temperatures for 18 strains of *Z. tritici*[44]. It was assumed that average cardinal temperature for each pathogen was identical across all hosts for each respective pathogen.

The Plantwise database (CABI) was used to estimate the host range of each pathogen in the Pathogen dataset. To improve matching of pathogen species names, some names were updated in the Plantwise database, according to the SFD or Mycobank (Supplementary Table 7). We also used host range information provided by ref. [16]. All plant–pathogen interaction records for hosts recorded in EarthStat (http://www.earthstat.org) and MIRCA2000 (ref. [34]) were extracted from the Plantwise database. To enable matching of host species, scientific names were assigned to plant hosts found in EarthStat and MIRCA2000 (Supplementary Table 6). The FAOSTAT commodity list (http://www.fao.org) was used to aid this process. Pathogens absent from the extracted plant–pathogen interaction dataset were excluded from the Pathogen dataset. Consequently, 80 pathogens were included in the Pathogen dataset and hence included in this study (Fig. 1 and Supplementary Table 1).

Estimating global distributions of pathogen hosts. Two approaches were used to estimate global host distributions for each pathogen included in the Pathogen dataset. First, for 150 crops (including forage crops; Supplementary Table 6), global estimates of average fractional proportion grid cell harvested (five-arc-minute spatial resolution) were obtained from EarthStat[33] (http://www.earthstat.org). Crops that could not be clearly identified as species (for example, 'mixed grain') or that contained a large number of plant genera (for example, 'vegetables') were excluded. Most crops classified as 'not elsewhere specified' were also excluded. For 150 crops, each crop map was converted to binary presence/absence. If the grid cell harvest area fraction was ≥0.00001 (equivalent to 0.1 m^2 ha^{-1}), the host was estimated as present in that grid cell. If the fraction was <0.00001, hosts were assumed absent. These values were chosen to ensure that crops were estimated as present in grid cells even if the average fractional proportion harvested was estimated as very small. This approach enabled the estimation of global distribution for each crop in EarthStat. The EarthStat crop distribution dataset does not provide crop calendars (that is, the months during which the crop is growing).

Second, for 22 crops (Supplementary Table 6), global estimates of growing season periods (around the year 2000) were extracted from MIRCA2000 at 30-arc-minute spatial resolution[34] and resampled to 5-arc-minute resolution using the neighbour-joining algorithm in the package raster for R (ref. [45]). For each crop, rainfed and irrigated growing season estimates were combined. This provided global monthly estimates of global host presence (within the growing season) and absence (outside the growing season), and hence monthly global distribution estimates, at 5-arc-minute spatial resolution for 22 crops.

For each pathogen, global distributions for all recorded hosts were combined and converted to binary presence/absence. This provided a single potential geographical distribution of each pathogen, based on reported pathogen host ranges (Plantwise) and geographic host distributions (EarthStat or MIRCA2000) (Supplementary Figs. 8 and 9). For example, if a pathogen was recorded in the Plantwise database to successfully infect four hosts recorded in EarthStat, any grid cells that were estimated to contain ≥1 of these hosts were converted to 1 (present), and grid cells that were estimated to contain 0 hosts were converted to 0 (absent). This was done independently for host distributions estimated from EarthStat and MIRCA2000, resulting in two alternative potential geographical distributions of each pathogen. Where MIRCA2000 was used, fewer pathogens were included, due to fewer crop species. Furthermore, where host range was estimated from MIRCA2000, the potential geographical range of a pathogen was estimated for each month, due to host growing season (Supplementary Fig. 9). Host ranges were assumed independent for each pathogen—that is, competition between pathogens for particular hosts was assumed to not occur.

Modelling pathogen temperature-dependent infection risk. Relative values of $r(T)$ were calculated by a beta function[46] (equation (1)) for each pathogen (Fig. 1 and Supplementary Table 1), for all climate data detailed above. We defined R_r as the number of pathogens with $r(T) \geq 0.5$—that is, those pathogens with high predicted infection rates. R_r acted as a summary metric of pathogen risk per grid cell:

$$r\left(T_{\{i,j\}}\right) = \left(\frac{T_{max} - T_{\{i,j\}}}{T_{max} - T_{opt}}\right)\left(\frac{T_{\{i,j\}} - T_{min}}{T_{opt} - T_{min}}\right)^{(T_{opt} - T_{min})/(T_{max} - T_{opt})} \quad (1)$$

where i is the month and j is the grid cell.

Model validation. Pathogen presence (defined as $r(T) \geq 0.5$) was calculated for recent average monthly temperature estimates using two alternative approaches. In the 'temperature-only' model, pathogens were not restricted by host distributions. In the 'temperature + host' model, pathogens were additionally restricted by host distributions estimated from EarthStat. In both model iterations, a summary potential global distribution of each pathogen was calculated, whereby if a pathogen was modelled as present in a grid cell during any month, then the pathogen was recorded as present in that grid cell.

Outputs from both model iterations were compared with observed records of pathogen presence at the country or state scale (hereafter collectively referred to as 'region', 396 regions total) from the CABI Plantwise database. Pathogen names in this dataset were updated according to the SFD or Mycobank to improve matching to the Pathogen dataset (Supplementary Table 7). Discovery and sanction author(s) of species were not provided in this dataset and so were not considered here. Thirteen pathogens (*Alternaria cucumerina*, *Botrytis cinerea*, *Cercospora carotae*, *Didymella arachidicola*, *Diplocarpon earlianum*, *Fusarium oxysporum* f.sp. *conglutinans*, *Fusarium roseum*, *Globisporangium ultimum*, *Nothopassalora personata*, *Puccinia menthae*, *Septoria glycines*, *Stigmina carpophila* and *Wilsoniana occidentalis*) were excluded from model validation due to an apparent lack of observational records.

Models were run at five-arc-minute resolution, whereas the observed pathogen records were at the regional scale (Supplementary Fig. 10a,c). Hence, the model outputs were summed to the regional scale (Supplementary Fig. 10b,d). If a pathogen was modelled as present in any grid cell in a region, for any month, the pathogen was modelled as present at the regional scale. GDP based on purchasing power parity (GDP (PPP)) and research output (number of publications) were obtained from the World Bank Data website for 230 territories (data.worldbank.org). For the temperature + host model, for each pathogen, median GDP (PPP) and median research output were calculated for territories where (1) both the temperature + host model estimated and the Plantwise database recorded a pathogen as present (true positive (sensitivity)), and (2) the temperature + host model estimated a pathogen as present, but the Plantwise database recorded a pathogen as absent (false positive (type 1 error)). The data were compared by Welch's two-sample two-tailed *t*-test. Where GDP (PPP) and research output were recorded at the country scale but pathogen records were recorded at the state scale, states were assigned country-level GDP (PPP) and research output.

Changes in global temperature-dependent infection risk. We calculated R_r for recent and future average monthly grid cell temperature ($T_{\{i,j\}}$) using two alternative host-restriction approaches. First, pathogens were restricted by host distributions estimated from EarthStat for each future climate scenario (RCPs 2.6, 4.5, 6.0 and 8.5). Second, pathogens were restricted by host distributions estimated

from MIRCA2000, and RCP 6.0 was used to estimate future average monthly temperature. This allowed for comparison between host restriction methods of model outputs of change in spatial patterns of R_t.

For each model, change in R_t was calculated as R_t under future climate conditions minus R_t under recent climate, for each grid cell for each month. Within a grid cell, increases or decreases in R_t do not reflect the change in species composition[7]. Therefore, for each model, a modified Jaccard (J) index ($1-J$) of community dissimilarity (pathogen turnover, equation (2))[7,47] was calculated to characterize the change in community composition in each grid cell for each month. High pathogen turnover indicates high community dissimilarity or a large change in species composition:

$$1 - J_{\{i,j\}} = 1 - \left(\frac{a_{\{i,j\}}}{a_{\{i,j\}} + b_{\{i,j\}} + c_{\{i,j\}}} \right) \quad (2)$$

where a is the number of pathogens common to a grid cell under recent and future climate, b is the number of pathogens unique to a grid cell under recent climate and c is the number of pathogens unique to a grid cell under future climate. Pathogen turnover was defined as zero for grid cells with no pathogens under both recent and future climates.

Comparison between future changes in crop yields and $r(T)$ by latitude. For each pathogen of each crop included in MIRCA2000, change in $r(T)$ between current and future climate (RCP 6.0) was calculated for each grid cell for each month (Supplementary Table 2 provides the number of pathogens included for each crop). Pathogens were restricted by crop distributions estimated from MIRCA2000 (see above). For this analysis, we used estimates from MIRCA2000 for pulses as a proxy for pea crop (*Pisum sativum*). For each crop–pathogen combination, the mean change in $r(T)$ was calculated for each latitude (five-arc-minute resolution) and then aggregated to 5° resolution for plotting using the aggregate function in package raster for R (ref. [45]) (Fig. 5).

We tested for evidence of spatial matching between projected changes in crop yield and pathogen $r(T)$. For each crop, Pearson correlations (r) and spatial cross-correlations (r_c) were calculated between the overall mean change in crop yield and pathogen $r(T)$, aggregated to 2° resolution. In this case, we compared the overall mean change in $r(T)$ for all months, for all pathogens with an overall mean change in yield from all available models under the no irrigation scenario. Spatial cross-correlations were calculated using the package spatialEco for R (ref. [48]). An inverse power law transformation was performed to derive a spatial weights matrix in the analysis of each crop.

Pathogen sampling bias. Northern and southern latitudinal ranges for plant pests and pathogens were extracted from the CABI Plantwise database. As previously described, some pathogen names in this dataset were updated according to the SFD or Mycobank to improve matching to the Pathogen dataset (Supplementary Table 7), and 13 pathogens were excluded from the analysis due to an apparent lack of observational records. Pathogen names were not updated in this dataset if they were absent from the Pathogen dataset. Northern and southern latitudinal ranges for pathogens included in the Pathogen dataset were compared with that of all fungal and oomycete pathogens for which latitudinal ranges were available.

Relative humidity considerations. Coupled Model Intercomparison Project 5 single-level monthly near-surface RH data (0.125° to 5° spatial resolution depending on the model) were extracted from the Climate Data Store (https://cds.climate.copernicus.eu). Data from all available future (RCP 6.0, 2070) and corresponding recent (1985) model–ensemble combinations (see Supplementary Table 8 for further details) were extracted from NetCDF files and converted to raster objects in R.

For each model–ensemble–month combination, change in RH was calculated as future RH minus recent RH. If a model had multiple ensembles, the mean change for each month was calculated from all ensembles. All data were resampled to five-arc-minute resolution using the bilinear algorithm in the package raster for R. The mean monthly change in RH was calculated from all model estimates to provide single monthly estimates. Grid cells that contained no hosts in the EarthStat database were excluded from the analysis. Hence, only grid cells included in analyses of R_t and pathogen turnover were included. Grid cells were aggregated to 2° spatial resolution to calculate Pearson correlations (r) between change in RH and change in R_t (RCP 6.0) for March, June, September and December.

The Appendix (Supplementary Information) compares $r(T)$ estimates from models using three-hourly temperature estimates constrained by leaf wetness with results obtained using only monthly average temperatures unconstrained by leaf wetness.

Reporting Summary. Further information on research design is available in the Nature Research Reporting Summary linked to this article.

Data availability

The fungal and oomycete cardinal temperature data are available in Dryad[42] (https://doi.org/10.5061/dryad.tqjq2bvw6) and from ref. [16]. The data on annual crop yield projections used in this study are from the Inter-Sectoral Model Intercomparison Project (https://www.isimip.org). The fungal and oomycete host plant data and geographical distributions (the Plantwise database) were used under license for the current study and are available with permission from CABI. The FAOSTAT commodity list is available from http://www.fao.org. The global gridded climate data and climate projections are available from WorldClim (https://www.worldclim.org). The global gridded crop distribution data used in this study are available from EarthStat (https://www.earthstat.org) and MIRCA2000 (https://www.uni-frankfurt.de/45218031/data_download). The fungal and oomycete names and name disambiguation data were obtained from Species Fungorum (http://www.speciesfungorum.org/) and MycoBank (http://www.mycobank.org/). The annual per capita GDP (PPP) data were obtained from the World Bank (https://data.worldbank.org/). Coupled Model Intercomparison Project 5 single-level monthly near-surface RH data were obtained from the Climate Data Store (https://cds.climate.copernicus.eu). Administrative boundaries for the maps were obtained from GADM (https://www.gadm.org). The coastal outlines were obtained from package rworldmap version 1.3–6 for R version 4.0.1.

Code availability

All analyses were conducted using existing functions for R version 4.0.1. No substantial custom code was used. R code used for data manipulation is available from the corresponding author on reasonable request.

References

35. Liu, J., Williams, J. R., Zehnder, A. J. B. & Yang, H. GEPIC—modelling wheat yield and crop water productivity with high resolution on a global scale. *Agric. Syst.* **94**, 478–493 (2007).
36. Liu, W. et al. Global investigation of impacts of PET methods on simulating crop–water relations for maize. *Agric. Meteorol.* **221**, 164–175 (2016).
37. Williams, J. R. & Sharpley, A. N. *EPIC—Erosion/Productivity Impact Calculator: 1. Model Documentation* (USDA, 1989).
38. Watanabe, M. et al. Improved climate simulation by MIROC5: mean states, variability, and climate sensitivity. *J. Clim.* **23**, 6312–6335 (2010).
39. Collins, W. J. et al. Development and evaluation of an Earth-system model—HadGEM2. *Geosci. Model Dev.* **4**, 1051–1075 (2011).
40. Dunne, J. P. et al. GFDL's ESM2 global coupled climate–carbon earth system models. Part I: physical formulation and baseline simulation characteristics. *J. Clim.* **25**, 6646–6665 (2012).
41. Dufresne, J.-L. et al. Climate change projections using the IPSL-CM5 Earth system model: from CMIP3 to CMIP5. *Clim. Dyn.* **40**, 2123–2165 (2013).
42. Bebber, D. P., Chaloner, T. M. & Gurr, S. J. *Fungal and Oomycete Cardinal Temperatures (the Togashi Dataset)* (Dryad, 2020); https://doi.org/10.5061/DRYAD.TQJQ2BVW6
43. Viswanath, K. et al. Simulation of leaf blast infection in tropical rice agro-ecology under climate change scenario. *Clim. Change* **142**, 155–167 (2017).
44. Boixel, A.-L., Delestre, G., Legeay, J., Chelle, M. & Suffert, F. Phenotyping thermal responses of yeasts and yeast-like microorganisms at the individual and population levels: proof-of-concept, development and application of an experimental framework to a plant pathogen. *Microb. Ecol.* **78**, 42–56 (2019).
45. Hijmans, R. J. et al. raster: Geographic data analysis and modeling. R package v.3.1-5 (2020).
46. Yan, W. & Hunt, L. A. An equation for modelling the temperature response of plants using only the cardinal temperatures. *Ann. Bot.* **84**, 607–614 (1999).
47. Wiens, J. A., Stralberg, D., Jongsomjit, D., Howell, C. A. & Snyder, M. A. Niches, models, and climate change: assessing the assumptions and uncertainties. *Proc. Natl Acad. Sci. USA* **106**, 19729–19736 (2009).
48. Chen, Y. A new methodology of spatial cross-correlation analysis. *PLoS ONE* **10**, e0126158 (2015).

Acknowledgements

T.M.C. is supported by BBSRC SWBio DTP studentship no. BB/M009122/1. D.P.B. and S.J.G. are supported by BBSRC grant no. BB/N020847/1 and the Global Burden of Crop Loss project (Bill and Melinda Gates Foundation). S.J.G. is supported by a CIFAR Fellowship, 'The Fungal Kingdom: Threats and Opportunities'.

Author contributions

D.P.B. and T.M.C. developed the concept, collated the data, conducted the analyses and prepared the figures. D.P.B. wrote the manuscript with contributions from T.M.C. and S.J.G.

Competing interests

The authors declare no competing interests.

Additional information

Supplementary information The online version contains supplementary material available at https://doi.org/10.1038/s41558-021-01104-8.

Correspondence and requests for materials should be addressed to D.P.B.

Peer review information *Nature Climate Change* thanks the anonymous reviewers for their contribution to the peer review of this work.

Reprints and permissions information is available at www.nature.com/reprints.

nature research

Corresponding author(s): Daniel Bebber

Last updated by author(s): Jun 11, 2021

Reporting Summary

Nature Research wishes to improve the reproducibility of the work that we publish. This form provides structure for consistency and transparency in reporting. For further information on Nature Research policies, see our Editorial Policies and the Editorial Policy Checklist.

Statistics

For all statistical analyses, confirm that the following items are present in the figure legend, table legend, main text, or Methods section.

n/a	Confirmed	
☐	☒	The exact sample size (*n*) for each experimental group/condition, given as a discrete number and unit of measurement
☒	☐	A statement on whether measurements were taken from distinct samples or whether the same sample was measured repeatedly
☐	☒	The statistical test(s) used AND whether they are one- or two-sided *Only common tests should be described solely by name; describe more complex techniques in the Methods section.*
☐	☒	A description of all covariates tested
☒	☐	A description of any assumptions or corrections, such as tests of normality and adjustment for multiple comparisons
☐	☒	A full description of the statistical parameters including central tendency (e.g. means) or other basic estimates (e.g. regression coefficient) AND variation (e.g. standard deviation) or associated estimates of uncertainty (e.g. confidence intervals)
☐	☒	For null hypothesis testing, the test statistic (e.g. *F*, *t*, *r*) with confidence intervals, effect sizes, degrees of freedom and *P* value noted *Give P values as exact values whenever suitable.*
☒	☐	For Bayesian analysis, information on the choice of priors and Markov chain Monte Carlo settings
☒	☐	For hierarchical and complex designs, identification of the appropriate level for tests and full reporting of outcomes
☒	☐	Estimates of effect sizes (e.g. Cohen's *d*, Pearson's *r*), indicating how they were calculated

Our web collection on statistics for biologists contains articles on many of the points above.

Software and code

Policy information about availability of computer code

Data collection	No software was used to collect data.
Data analysis	Data analyses were conducted in R version 4.0.1

For manuscripts utilizing custom algorithms or software that are central to the research but not yet described in published literature, software must be made available to editors and reviewers. We strongly encourage code deposition in a community repository (e.g. GitHub). See the Nature Research guidelines for submitting code & software for further information.

Data

Policy information about availability of data

All manuscripts must include a data availability statement. This statement should provide the following information, where applicable:

- Accession codes, unique identifiers, or web links for publicly available datasets
- A list of figures that have associated raw data
- A description of any restrictions on data availability

Fungal and oomycete cardinal temperature data are available in Dryad https://doi.org/10.5061/dryad.tqjq2bvw6 and from Magarey, R. D., Sutton, T. B., & Thayer, C. L. (2005). A Simple Generic Infection Model for Foliar Fungal Plant Pathogens. Phytopatholog 95(1), 92–100. https://doi.org/10.1094/PHYTO-95-0092.
The annual crop yield projections data used in this study the Inter-Sectoral Model Intercomparison Project (ISIMIP), https://www.isimip.org
Fungal and oomycete host plant data and geographical distributions (the Plantwise database) were used under license for the current study, and are available with permission from CABI, Wallingford, UK.
The FAOSTAT commodity list is available from http://www.fao.org
Global gridded climate data and climate projections are available from https://www.worldclim.org
Global gridded crop distribution data used in this study are available from EarthStat https://www.earthstat.org and MIRCA2000 https://www.uni-

frankfurt.de/45218031/data_download
Fungal and oomycete names and name disambiguation data were obtained from Index Fungorum http://www.indexfungorum.org/ and associated Species Fungorum http://www.speciesfungorum.org/ as well as MycoBank http://www.mycobank.org/
Annual per capita GDP at purchasing power parity (PPP) data were obtained from the World Bank https://data.worldbank.org/
CMIP5 single level monthly near surface relative humidity data were obtained from the Climate Data Store (https://cds.climate.copernicus.eu).
Administrative boundaries for maps were obtained from GADM (https://www.gadm.org). Coastal outlines were obtained from package rworldmap version 1.3-6 for R version 4.0.1.

Field-specific reporting

Please select the one below that is the best fit for your research. If you are not sure, read the appropriate sections before making your selection.

☐ Life sciences ☐ Behavioural & social sciences ☒ Ecological, evolutionary & environmental sciences

For a reference copy of the document with all sections, see nature.com/documents/nr-reporting-summary-flat.pdf

Ecological, evolutionary & environmental sciences study design

All studies must disclose on these points even when the disclosure is negative.

Study description	This study compared changes in global agriculture of 12 major crops and plant pathogenic fungi and oomycete infection risk under climate change. This study utilised available data concerning annual crop yield projections, pathogen cardinal temperature, pathogen host plant interactions and geographical distributions, global gridded climate data and climate projections, global gridded crop distributions, and GDP PPP data.
Research sample	This study was based on available data concerning crop hosts, pathogens, climate change, and GDP. Fungal and oomycete cardinal temperature data are available in Dryad https://doi.org/10.5061/dryad.tqjq2bvw6 and from Magarey, R. D., Sutton, T. B., & Thayer, C. L. (2005). A Simple Generic Infection Model for Foliar Fungal Plant Pathogens. Phytopatholog 95(1), 92–100. https://doi.org/10.1094/PHYTO-95-0092. The annual crop yield projections data used in this study the Inter-Sectoral Model Intercomparison Project (ISIMIP), https://www.isimip.org Fungal and oomycete host plant data and geographical distributions (the Plantwise database) were used under license for the current study, and are available with permission from CABI, Wallingford, UK The FAOSTAT commodity list is available from http://www.fao.org Global gridded climate data and climate projections are available from https://www.worldclim.org Global gridded crop distribution data used in this study are available from EarthStat https://www.earthstat.org and MIRCA2000 https://www.uni-frankfurt.de/45218031/data_download Fungal and oomycete names and name disambiguation data were obtained from Index Fungorum http://www.indexfungorum.org/ and associated Species Fungorum http://www.speciesfungorum.org/ as well as MycoBank http://www.mycobank.org/ Annual per capita GDP at purchasing power parity (PPP) data were obtained from the World Bank https://data.worldbank.org/ CMIP5 single level monthly near surface relative humidity data were obtained from the Climate Data Store (https://cds.climate.copernicus.eu). Administrative boundaries for maps were obtained from GADM (https://www.gadm.org). Coastal outlines were obtained from package rworldmap version 1.3-6 for R version 4.0.1.
Sampling strategy	No sample size calculations were performed. Sample sizes were determined by available data in the various data sources utilised in this publication.
Data collection	Fungal and oomycete cardinal temperature data, global gridded climate data and climate projections, global gridded crop distribution data, and fungal and oomycete names and name disambiguation data were collected by TMC. Annual crop yield projections data, GDP PPP data, and the Plantwise database were collected by DPB.
Timing and spatial scale	All relevant time scales relating to when data were collated and processed are provided in the Methods section of this study.
Data exclusions	Global estimates of average fractional proportion grid cell harvested (5 arc minute spatial resolution) were obtained from EarthStat (http://www.earthstat.org) for 150 crops. Crops that could not be clearly identified as species (e.g. “mixed grain”) or contained a large number of different plant genera (e.g. “vegetables”) were excluded. Most crops classified as “not elsewhere specified” (nes) were also excluded. Table S6 details crops used in this analysis. All full list of available crop distributions are available from EarthStat (http://www.earthstat.org). Thirteen pathogens (Alternaria cucumerina, Botrytis cinerea, Cercospora carotae, Didymella arachidicola, Diplocarpon earlianum, Fusarium oxysporum f.sp. conglutinans, Fusarium roseum, Globisporangium ultimum, Nothopassalora personata, Puccinia menthae, Septoria glycines, Stigmina carpophila, and Wilsoniana occidentalis) were excluded from model validation and pathogen sampling bias analyses, due to an apparent lack of observational records.
Reproducibility	The study did not use experiments, but collated and analysed preexisting available data. Therefore, no measures to ensue reproducibility were implemented. However, all data utilised in this study are either provided, freely available from the relevant referenced literature/sources, or available from CABI (upon request), to reproduce results reported here. See Data Availability statement for further details.

Randomization	No randomization was performed.
Blinding	This was not an experimental study, hence blinding was not necessary.

Did the study involve field work? ☐ Yes ☒ No

Reporting for specific materials, systems and methods

We require information from authors about some types of materials, experimental systems and methods used in many studies. Here, indicate whether each material, system or method listed is relevant to your study. If you are not sure if a list item applies to your research, read the appropriate section before selecting a response.

Materials & experimental systems

n/a	Involved in the study
☒	☐ Antibodies
☒	☐ Eukaryotic cell lines
☒	☐ Palaeontology and archaeology
☒	☐ Animals and other organisms
☒	☐ Human research participants
☒	☐ Clinical data
☒	☐ Dual use research of concern

Methods

n/a	Involved in the study
☒	☐ ChIP-seq
☒	☐ Flow cytometry
☒	☐ MRI-based neuroimaging